Quantum and semi-classical transport in NEMO 1-D

Gerhard Klimeck
Jet Propulsion Laboratory, California Institute of Technology, Pasadena CA 91109
gekco@jpl.nasa.gov

Abstract. **The coupling of the fundamentally quantum mechanical nanoelectronic transport simulation through resonant tunneling diodes to semi-classical drift diffusion in the contacts is demonstrated. The coupling between the non-equilibrium Green function formalism used in NEMO to the drift diffusion equation is established by the use of spatially dependent quasi Fermi levels in the reservoirs. The charge distributions are computed quantum mechanically throughout the whole device using full bandstructure sp3s* tight binding model that includes band non-parabolicity and band warping. The formalism is applied to the simulation of high current density resonant tunneling diodes. Low mobility contacts are shown to introduce a bi-stability in the negative differential resistance region.**

Key Words. ***Transport, classical, quantum, tunneling, diffusion.***

1. Introduction

NEMO 1-D has been developed [1] primarily for the simulation of resonant tunneling diodes (RTDs), and quantitative and predictive agreements with experimental high performance, high current density devices have been achieved in the past [2, 3]. There are four key ingredients to the success of these simulations: 1) the treatment of the extended contacts including quasi bound states and empirical relaxation time approximation scattering with a surface Green function, 2) accurate description of bandstructure using empirical tight binding models, 3) quantum charge self-consistency including a Hartree and exchange potential, and 4) the proper numerical integration over the transverse momentum.

The treatment of the contacts assumes that the device is subdivided into three distinct regions: 1/2) a left/right reservoir in local equilibrium with the left/right contact with well established left/right quasi-Fermi levels, and 3) a central device region which is treated to be in non-equilibrium using the non-equilibrium Green function formalism (NEGF). The central device region is considered to be the current limiting element in the device. The left/right reservoirs are assumed to be in local equilibrium with a flat Fermi level and conductive enough to provide current without depletion of the reservoir. Despite the successful comparisons to experiments one question remained lingering in the treatment of the reservoirs: How good is the assumption of a local equilibrium or how good is the assumption of a flat Fermi level? The expansion of the NEMO 1-D code to couple a drift-diffusion model in the reservoirs to the central non-equilibrium region addresses these questions.

2. Drift Diffusion Formulation

The drift diffusion equation can be formulated [4] such that the electron current density, J, in a particular device region is proportional to the site (i) dependent mobility, μ_i, electron density, n_i, and the gradient of the quasi electron Fermi energy, $E_{F,i}$, with $J = \mu_i n_i \nabla E_{F,i}$. Hole current and recombination or generation effects are neglected in work. The expression holds for an arbitrary density of states for arbitrary electron distributions. This independence enables the coupling of an electron density that is computed in a quantum mechanical full bandstructure model that includes the proper treatment of quasi-bound states in the emitter. Current is computed in the central non-equilibrium region only and imposed on the whole device. The drift diffusion equation is solved iteratively in the reservoir regions only. The drift diffusion equation therefore influences the Fermi level, which in turn influences the injected current in the central device, the charge distribution, and electrostatic potential through the iterative solution of the Poisson equation and the NEGF transport equations. The mobility is assumed to be constant throughout the contacts for simplicity in these fist demonstration simulations. The advantage of this approach over the one presented in reference [5] is our use of our surface green function boundary condition which can properly model extended contact regions[6].

3. Simulations

The example structure used here is the same as the standard unstrained InGaAs/InAlAs RTD on InP subtrate from the NEMO test matrix described in reference [3]. The barriers and well have a nominal thickness of 16 monolayers (4.69nm) and are clad by 1.76 nm of undoped buffer ($2\times10^{16}cm^{-3}$), a 50nm low

doping buffer of $9x10^{17}cm^{-3}$ and $5x10^{18}cm^{-3}$ doped contacts.

The actual simulations use a well width of 18 monolayers that was derived in a simpler bandstructure single band model through genetic algorithm fitting [7]. Here a full band sp3s* bandstructure model with numerical integration over the transverse momentum with complete charge self-consistency is used. The numerical integration in energy E and momentum k inside the Hartree self-consistency loop was enabled for practical turn-around times by the efficient parallelization of the NEMO code [8].

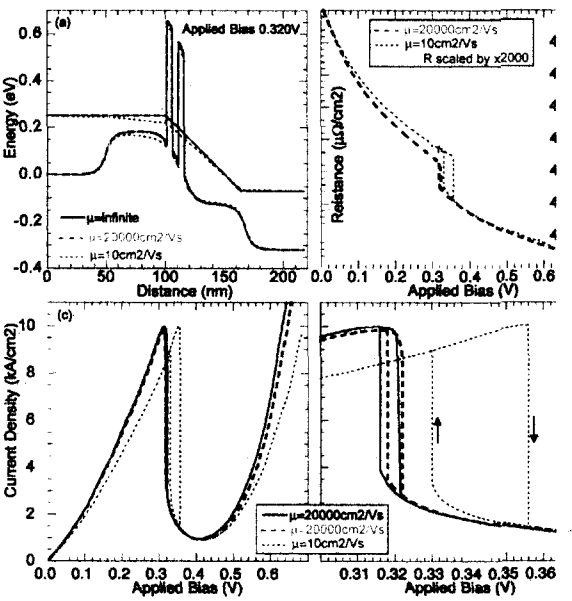

Fig. 1. Comparison of three classical transport models in the contacts: infinite mobility, mobility 20,000cm2/Vs and 10cm2/Vs. (a) Conduction band profileCurrent Voltage characteristics computed with three classical transport models in the contacts: infinite mobility, mobility 20,000cm2/Vs and 10cm2/Vs. (a) full forward and reverse voltage sweeps indicating regions of bi-stability around the current turn-off. (b) zoom of (a).

Figure 1 illustrates the effects of the introduction of a finite mobility in the contacts on the potential profiles, Fermi levels, and current voltage characteristics (I-Vs). Three cases are compared in particular: no drift diffusion model in the contacts (infinite mobility) and mobilities of $20{,}000cm^2/Vs$ and $10cm^2/Vs$.

Figure 1a) compares the conduction band edge and Fermi level for the three cases at a bias of 0.32V. The non-equilibrium region extends over the central device region and the low doping buffer region (100-160nm) as indicated by the interrupted quasi Fermi level in that region. This quasi Fermi level is not utilized in the non-equilibrium region and the drift-diffusion equation is only solved in the left and right contact (0-100nm, 160-220nm, respectively). A resistor-like drop in the potentials in the emitter is visible the lower mobility case while the high mobility and simulation look virtually identical.

Figures 1c) and 1d) compare the computed current voltage characteristics (I-Vs) for the three simulation cases. The high mobility case is virtually identical to the infinite mobility case. A forward and reverse bias sweep in the positive voltage axis shows a bi-stability in the negative differential resistance region of these I-V characteristics of 4mV. The low mobility case shows a significantly increased bi-stability region of 26meV. The bias region of bi-stability is shown expanded in Figure 1d).

The increased bi-stability region can be intuitively explained by the introduction of a series resistance where $V_C=RI+V_D$ where V_C is the external contact voltage, V_D the voltage drop over the central device, R the series resistance and I the current. The peak-to-valley current swing from ~9.9kA/cm2 to ~2.5kA/cm2 to at the turn-off of the RTD at the intrinsic device voltage of V_D~0.32V requires series resistance of about $R=26mV/7.4kA/cm^2=3.5\mu\Omega/cm^2$ to induce bi-stability of 26mV.

Figure 1b) shows the resistance caused by the introduction of finite mobility as a function of bias. The resistance is here defined as the total drop of the Fermi level in the left and the right contact divided by the total current. The average value of about $4.4\mu\Omega/cm^2$ compares reasonably well to the estimate from the bi-stability argument. However, since the introduction of a finite mobility changes the peak current from $9.8kA/cm^2$ to $10.0kA/cm^2$ the overall effect in the device is more complicated than a simple series resistance voltage drop. Also the resistance is not constant over the voltage range and shows a discontinuity at the RTD turn-off. The discontinuity can be associated with reactive equivalent circuit components [9-11]. There is an intricate interplay between the non-linear charge distribution, Fermi level and current density in the device. The following figures illustrate this interdependence.

Figure 2 analyzes the band profiles, Fermi levels and charge distributions for the forward and reverse voltage sweep of the high mobility ($20{,}000cm^2/Vs$) simulation in its bi-stability region at a bias of 0.32V. The forward sweep of the low mobility ($10cm^2/Vs$) simulation is shown for reference in some plots as well. Figure 2a shows the overall potential profile similar to Figure 1a). A difference in the forward and reverse bias sweep can only be identified in the in the more detailed plot of Figure 2b) in the very center of the RTD. This potential difference can be traced to the charge filling of the central resonance which is depicted in Figures 2c) and 2d). The high current state (forward sweep) shows significantly more charge in the well indicating charge accumulation. In the reverse sweep the well is empty and charge accumulated in

front of the RTD. Indeed the low current state chows a larger charge than the high current state in the triangular notch region of 90-100nm.

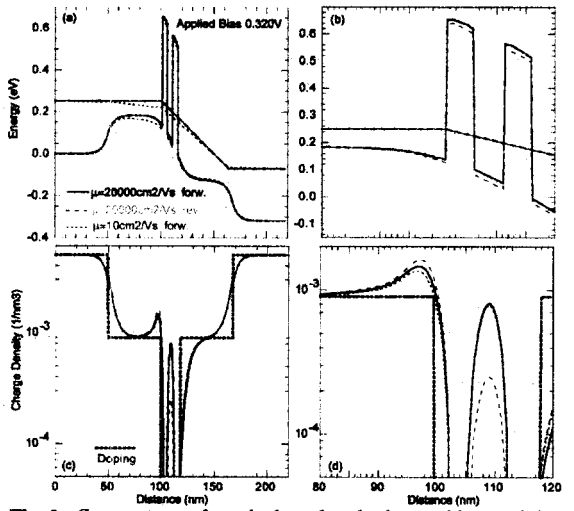

Fig. 2. Comparison of results based on high a and low mobility solutions (20,000cm²/Vs and 10cm²/Vs) at a bias of 0.32V. (a) Conduction band profile. (b) zoom of (a) around the central RTD. (c) and (d) corresponding electron distribution and doping profile.

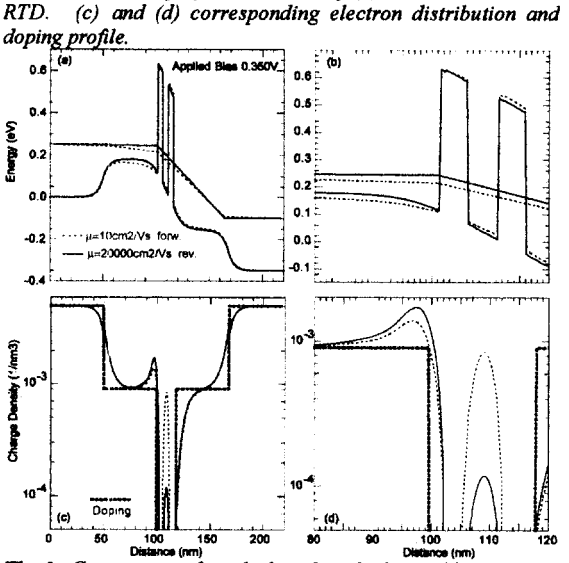

Fig. 3. Comparison of results based on high a and low mobility solutions (20,000cm²/Vs and 10cm²/Vs) at a bias of 0.35V. (a) Conduction band profile. (b) zoom of (a) around the central RTD. (c) and (d) corresponding electron distribution and doping profile.

Charge is computed quantum mechanically in the full bandstructure model in the low doping region from about 50nm to 170nm. In the high doping regions the charge is computed semi-classically in a Thomas-Fermi model. This enables the proper treatment of the quasi-bound states in the emitter and the proper treatment of the charge in that region. It is interesting to note here that the low mobility solution at this bias has a charge distribution that is virtually identical to the high current state of the high mobility solution, yet the current at that voltage is about 20% lower in the low mobility case.

Figure 3 sheds more light on the low mobility simulation for the forward and reverse bias sweep in its bi-stability region at a voltage of 0.35V. Both sweeps show a potential drop in the Emitter Fermi level and a significant modulation of the conduction band edge compared to the high mobility case discussed in Figure 2. The electrostatic potential difference is not in the high and low current state is no longer confined to the central RTD region, but extends significantly into the emitter region. The origin of the potential difference is the charge self-consistent simulation coupled to the spatially varying Fermi level in the emitter. The high current state forces a significantly larger Fermi level drop than he low current state. The potential in the emitter adjusts accordingly.

4. *Experiment Comparison and Discussion*

Figure 4 compares four experimental I-V curves taken from two different devices off different wafers with the positive and negative voltage results on the same positive voltage axis to the three simulation cases studied so far. The insert in Figure 4 shows the experimental data alone for clarity. Although the two devices are nominally the same, they do show slightly different characteristics that may be related to structural deviations or doping profile deviations from the original device specifications. Positive and negative voltage sweeps show virtually identical results indicating a very good symmetry in the device. Barrier or doping asymmetries would show asymmetries in the forward and reverse voltage sweeps [3]. The peak current density difference could be attributed to a barrier thickness variation or doping variation from one wafer / device to the other.

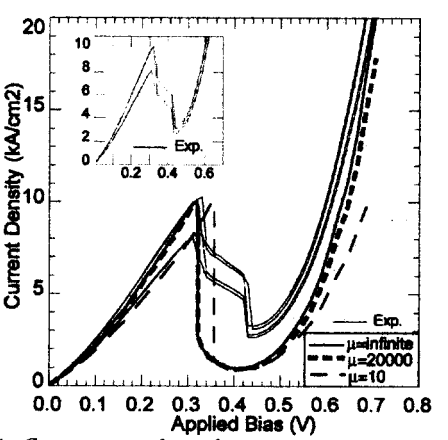

Fig. 4. Comparison of simulations to experimental data. Inset shows experimental data only for clarity.

Within the margins of the model the new simulations follow nicely the experimental data. The

high mobility curves follow closely the higher current device. The low doping curve follows the lower current density device. However the high bias turn-on shows a significant deviation from the experimental data. Deviations within the high bias regions can be attributed to the details of the bandstructure model and its non-parabolicity as discussed in [12].

Deviations in the simulation from the experimental data can in principle also be attributed to our limited detailed structural knowledge of the devices. In the simulations here we are using the barrier and well thickness and doping profile as extracted from a genetic parameter fitting with a genetic algorithm [7]. The bandmodel used in those simulations was single band numerical extraction of the full band sp3s* model. The mapping of the non-parabolicity and band warping is not perfectly identical and simulation may have slightly different results. Decreasing the barrier width by one monolayer may raise the valley current and the second state current turn-on to provide better fit with the low mobility included in the simulation.

5. *Discussion on Bi-Stability*

The original measurements of these devices were performed by Ted Moise at Texas Instruments in 1995 who ensured the NEMO team that the steps in the NDR region are purely due to external circuitry oscillations and he provided the team with a set of measurements that showed no bi-stability at all. The author has, however no longer access to these data. The valley current is underestimated by a factor of about 2.5. NEMO results have shown that the introduction of exchange and correlation and the introduction of scattering [13] as well as the introduction of full bandstructure models [8] reduce the bi-stability observed numerically in simulations of nominally symmetric structures. The scattering mechanism and transport through non-parabolic bandstructure models increases the valley current, increases the stored charge in the quantum well in the off state and therefore reduces the associated potential swing in the central device. It is the author's opinion that the introduction of the proper scattering will increase the charge in the turn-off region enough to eliminate the reagion of bi-stability.

6. *Conclusion*

A realistic drift-diffusion model was included in the NEMO 1-D simulation tool to analyze the effects of finite conductance in the electron reservoirs that surround the central tunneling region. The introduction of finite conductivity in the reservoirs does not provide significant new insight into the transport of the high current density devices studied here. The assumption of a well defined reservoir with flat Fermi levels appears to work well for this class of devices. However lower doping devices with longer buffer layers may benefit from the improved reservoir treatment.

Acknowledgments

The work described in this publication was carried out at the Jet Propulsion Laboratory, California Institute of Technology under a contract with the National Aeronautics and Space Administration. The supercomputer used in this investigation was provided by funding from the NASA Offices of Earth Science, Aeronautics, and Space Science. I would like to acknowledge Drs. R. Chris Bowen and Phillip Stout for their help in the early prototypes of the coupled drift diffusion and NEGF transport model within a single band model. I would also like to acknowledge fruitful collaborations that lead up to this work within the core NEMO team consisting of Dr. R. Chris Bowen, Dr. Roger Lake and Dr. Timothy B. Boykin. I would also like to thank T. Wack for the review of the manuscript.

References

1. Lake, R., et al., *Single and multiband modeling of quantum electron transport through layered semiconductor devices.* J. Appl. Phys., 1997. **81**(12): p. 7845-7869.
2. Blanks, D., et al., *NEMO: General release of a new comprehensive quantum device simulator.* Comp. Semic. 1997, 1998. **156**: p. 639-642.
3. Klimeck, G., et al., *Quantitative Simulation of Strained InP-Based Resonant Tunneling Diodes.* IEEE DRC, 1997: p. 92.
4. Pierret, R.F., *Advanced Semiconductor Fundamentals.* Modular Series on Solid State Devices, ed. R.F. Pierret and G.W. Neudeck. Vol. Volume VI. 1989.
5. Daniel, E.S., et al., *Coupled drift-diffusion/quantum transmitting boundary method simulations of thin oxide devices with specific application to a silicon based tunnel switch diode.* IEEE Trans. on Electr. Dev, 2000. **47**(5): p. 1052-1060.
6. Klimeck, G., et al., *Quantum device simulation with a generalized tunneling formula.* Appl. Phys. Lett., 1995. **67**(17): p. 2539--2541.
7. Klimeck, G., et al., *"Genetically Engineered" Nanostructure Devices.* Proc. Mat. Res. Soc., 1998. **551**: p. 149.
8. Klimeck, G., *Parallelization of the Nanoelectronic Modeling Tool (NEMO 1-D) on a Beowulf Cluster.* J. of Computational Electr., 2002. **1**(1-2): p. 75-79.
9. Schulman, J.N., H.J.D.L. Santos, and D.H. Chow, *Physics-based RTD current-voltage equation.* Electr. Dev. Lett., 1996. **17**: p. 220-222.
10. Broekaert, T.P.E., et al., *A monolithic 4-bit 2 GPPS resonant tunneling analog-to-digital converter.* IEEE J. Solid State Circuits, 1998. **33**(9): p. 1342-1349.
11. Lake, R. and J. Yang, *A Physics Based Model for the RTD Quantum Capacitance.* IEEE Trans. on Electr. Dev., 2003. **to appear**.
12. Bowen, R., et al., *Quantitative simulation of a resonant tunneling diode.* J. Appl. Phys., 1997. **81**(7): p. 3207-3213.
13. Klimeck, G., R. Lake, and D.K. Blanks, *Role of interface roughness scattering in self-consistent resonant tunneling diode simulation.* Phys. Rev. B, 1998. **58**: p. 7279.